Evidence of superdiffusive nanoscale motion in anionic polymeric hydrogels: Analysis of PGSE- NMR data and comparison with drug release properties

Franca Castiglione[a,*], Mosè Casalegno[a,*], Monica Ferro[a], Filippo Rossi[a], Guido Raos[a], and Andrea Mele[a,b]

a Department of Chemistry, Materials and Chemical Engineering "Giulio Natta", Politecnico di Milano, Via Mancinelli 7, 20131 Milan, Italy;

b CNR Istituto di Chimica del Riconoscimento Molecolare, Via Mancinelli 7, 20131 Milan, Italy

*Corresponding authors, email: franca.castiglione@polimi.it, mose.casalegno@polimi.it

Abstract

Polymeric hydrogels are promising candidates for drug delivery applications, thanks to their ability to encapsulate, transport and release a wide range of chemicals. The successful application of these materials requires a deep understanding of the mechanisms governing solute transport at the nanoscale and its impact on release kinetics. In this work, we investigate the translational diffusion of ibuprofen loaded in anionic agarose-carbomer (AC) hydrogels by ^{1}H high resolution magic angle spinning (HR-MAS) NMR spectroscopy, and compare it to its macroscopic release kinetics. The analysis of the experimental NMR data provides the first evidence of superdiffusion for ibuprofen in AC hydrogels. Superdiffusive transport is observed in the majority of our samples, especially those with the smallest mesh size (7 nm) and highest ibuprofen concentrations (90-120 mg/mL). This outcome is rationalized in terms of heavy-tailed distributions of spatial displacements (Lèvy flights) and of waiting times, which depend on the nanoscopic structural heterogeneity of the gels and the strong but reversible association between ibuprofen and the agarose matrix.

Keywords: drug delivery, hydrogels, anomalous diffusion, PGSE-NMR spectroscopy.

1. Introduction

Hydrogels are three-dimensional, water-swollen polymer networks. [1-3] Although water-insoluble due to strong physical or chemical cross-linking, hydrogels may retain large amounts of water, thus providing a versatile matrix with tissue-like mechanical properties. [4] Thanks to these features, hydrogels have found applications in the area of tissue engineering, [5] biosensors, [6,7] chemical analysis, [8] agriculture, [9] and drug delivery. [10-15] The latter application involves the use of hydrogels to deliver pharmaceuticals into the body, where they can be subsequently released in a controlled way. Hydrogels are extremely versatile, [16-18] and their porous structure can be easily modified, for example by changing the cross-linking density, to load and transport pharmaceuticals to specific target tissues. [19] Hydrogel-based products can be prepared in a variety of different formulations, spanning a wide range of drug administration routes. [11,15,20-25]

One important feature of hydrogels is related to the possibility to develop controlled drug release devices. The term "controlled release" refers to the ability of a system to maintain the drug concentration at an optimal value in the target tissues over an extended period of time, avoiding under-and overdosing problems. [15,26] Ideally, the release rate should also be constant over time so to prevent excessive accumulation or depletion, which may increase the risk of side effects or significantly limit drug effectiveness.

Despite significant progress in designing hydrogel-based systems for drug delivery, [27-29] the optimization and characterization of drug release properties remain challenging and require a deep understanding of the mechanisms regulating molecular transport within the gel matrix. [30] Factors such as hydrogel swelling and matrix degradation have a significant impact on both release and transport properties. Hence, non-degradable, swollen hydrogels are ideal candidates to investigate the relationship between release and transport properties. In such hydrogels, drug release is essentially diffusion-controlled. The driving force for drug release is, in this case, the solute concentration gradient (or, more generally, the chemical potential gradient) existing between the hydrogel and the release medium. In the simplest case, the net flux of drug leaving the hydrogel would be directly proportional to the concentration gradient through a numerical constant, i.e. the solute diffusion coefficient. This relationship, known as Fick's first law, has provided the starting point for the development of a number of mathematical models [4,31-33] to predict drug release from solute diffusion data. In many cases, such equations, including Higuchi's [34] one, have also been used reversely, i.e. to estimate solute diffusion coefficients from experimental release data, or to infer the solute transport mechanism. [32,35] In some cases, [33,36,37] the diffusion coefficients obtained by this approach have been successfully compared with experimental ones. Nonetheless,

due to the time scale of release experiments (typically minutes/hours), such estimates alone cannot be expected to clarify the mechanisms of solute transport on the molecular scale.

Many experiments have demonstrated the notable structural nanoscopic complexity of hydrogels. [38] First of all, like any polymer network such as vulcanized rubber, they can be characterized by a cross-linking density X, or alternatively by an average mesh size $\xi \propto -1/3$. This affects their elastic modulus and their swelling equilibrium. In fact, ξ is typically measured from the latter, exploiting the Flory-Rehner model for the free-energy of a swollen network. In addition, many light- and small-angle X-ray or neutron scattering experiments have highlighted the existence of strong, effectively frozen concentration fluctuations at length scales significantly larger than the mesh size. Depending on the specific chemistry of each system and the experimental conditions, these features may be interpreted in terms of cross-linking inhomogeneities, swelling inhomogeneities leading to solvent-rich cavities and polymer-rich bundles, or by a microphase separation between the different polymeric components of the gel. In any case, some large-scale structural heterogeneities can be expected to be almost ubiquitous in polymeric gels, [39] also according to statistical-mechanical analyses (see ref. 40, for example).

The structural heterogeneity of hydrogels should influence also their drug diffusion and release properties. Diffusive transport mainly occurs within the water-rich regions of the gels and it is known to depend on many factors such as solute concentration, degrees of gel swelling and cross-linking density, and solute-polymer interactions. [41-44] In relatively homogeneous hydrogels with large meshes, weak solute-polymer interactions, and negligible viscoelastic relaxation, the translational motion of solute can still be regarded as Fickian. Generally, the so-called Fickian motion implies a single, constant diffusion coefficient and a mean-square displacement scaling linearly with time. This kind of motion is often associated with an underlying Gaussian probability distribution of the molecular displacements, [45] although several exceptions have been reported of non-Gaussian, yet Fickian transport regimes. [46,47] In many other diffusion-controlled systems where the above conditions are not met, significant deviations have been observed, leading to an anomalous transport behavior. [45,48]

Anomalous dynamics is ubiquitous in soft condensed matter, and has been reported in a wide variety of systems, [47,49] including hydrogels. [50,51] Lèvy flights models [52-54] have attracted a considerable deal of interest, due to their ability to describe a number of anomalous superdiffusive phenomena (see below). Such models encompass a broad class of continuous random walk processes characterized by “heavy-tailed” displacement distribution probabilities in both space and time. Lèvy particle motion is thus characterized by large spatial displacements (jumps) and long waiting times (sojourns), violating the conditions for validity of the central limit theorem which leads to ordinary Gaussian diffusion.

Among the experimental techniques able to monitor solute diffusion in hydrogels, [55-61] pulse gradient spin echo NMR (PGSE-NMR) has proven especially valuable, as it offers the possibility to investigate the translational dynamics of small molecules non-invasively and quantitatively, [36,62,63] also in presence of nanoscale confinement. Importantly, this technique can be applied to drug-loaded hydrogels in thermal equilibrium, with no need of drug concentration gradients. PGSE-NMR also benefits of approaches specifically designed to identify restricted diffusion phenomena in soft materials. One of them, the q-space approach, [64,65] has widely been applied to analyze NMR data in soft tissues, [66] yet its application to hydrogels has so far been limited. [67,68] In soft materials, such as gels [69] and swellable solids, [70] high resolution (HR) spectra can be obtained using a magic angle spinning (MAS) setup. The enhanced spectral quality is mainly due to the MAS system, which minimizes the sample heterogeneity and anisotropic NMR interactions (such as chemical shift anisotropy and homonuclear dipolar couplings) that are usually observed in non-liquid samples. Several applications of HR-MAS combined with PGSE-NMR technique to the study of whole cells, tissues and polymers have been reported in literature, following the pioneering work of Shapiro [71] and Alam [70,72].

In this work, we use the PGSE-NMR technique to characterize the translational diffusion of ibuprofen in anionic agarose-carbomer (AC) hydrogels (carbomer is a commercial name for poly(acrylic acid)). [73] In particular, we consider the effect of drug concentration and hydrogel nanoscopic mesh size on ibuprofen transport properties. Our interest in these systems is motivated by the importance of ibuprofen as inflammatory drug [74-76] and the applicability of AC hydrogels for ibuprofen delivery. Besides, being non-degradable and non-swelling, AC hydrogels are ideally suited to assess the role of diffusion in release kinetics. The NMR results for the ibuprofen diffusivities are compared with macroscopic measurements of the kinetics of drug release by the hydrogels.

2. Materials and methods

2.1 Materials

Carbomer 974P (CAS 151687-96-6) with high molecular weight (about 1 MDa) was provided by Fagron (The Netherlands), triethylamine (TEA, CAS 121-44-8) with high purity was purchased from Fluka (Switzerland), while propylene glycol (CAS 504-63-2) and glycerol (CAS 56-81-5) were provided by Sigma-Aldrich (Germany). Phosphate Buffer Saline solution (PBS), purchased from Sigma-Aldrich (Germany), was used as solvent. Deuterated PBS was used for spectroscopic analysis in order to avoid overlapping of ^{1}H signals. The other polymer involved in the reaction is agarose (CAS 9012-36-6), purchased from Invitrogen (USA) and having a molecular

weight of about 300 kDa. Lastly, ibuprofen sodium salt (IBU, CAS 31121-93-4) was provided by Sigma-Aldrich (Germany). All materials were used as received.

2.2 Hydrogel synthesis and drug loading

Carbomer 974P, glycerol and propylene glycol were stirred together in a deuterated PBS solution, and the pH of the resulting mixture was neutralized with TEA. Agarose powder was subsequently added and the system was electromagnetically heated to initiate condensation reactions. Ibuprofen was added to the polymeric formulate as aqueous solution, before the cross-linking procedure and thus before the sol/gel transition occurred. Loading concentrations were 30, 60, 90, and 120 mg/mL. The 30 mg/mL samples were only used in release experiments (see below). The gelling solutions were then placed in steel cylinders (0.5 mL each) and left to rest until the achievement of complete gelation and thermal equilibrium. [77] The formation of ester bonds between agarose and carbomer, which leads to the formation of the hydrogel networks, was described in previous works [78], where agarose-carbomer based hydrogels were first introduced.

In the present study, we considered four different hydrogel formulations, hereafter abbreviated as AC1, AC2, AC4, and AC6. Details about their chemical composition and structure are provided in Table 1. The structure of a hydrogel can be quite complex, as it depends on the functionality and density of the cross-links, the distribution of polymer strand lengths between the cross-links, and their degree of swelling. The simplest structural descriptor is the mesh size ξ, which corresponds the average distance between the cross-links and can be estimated from solvent uptake experiments according to the Flory-Rehner (F-R) theory [79]. More specifically, $\xi \propto Q_V^{1/3}$ where Q_V is the volumetric swelling ratio. An overview of the F-R theory and its application to AC hydrogels is given in our previous works. [80] However, as argued by one of the reviewer, an issue of insufficient accuracy of the experimental determination of ξ by the F-R methods highlighted above can be raised. An improved experimental approach to the measurement of ξ in polymeric hydrogels was proposed on the basis of SANS data [B. Rossi, A. Paciaroni, V. Venuti, G. C. Fadda, L. Melone, C. Punta, V. Crupi, D. Majolino, A. Mele, “SANS investigation of water adsorption in tunable cyclodextrin-based polymeric hydrogels” *Phys. Chem. Chem. Phys.* **2017,** *19*, 6022-6029] but not tested yet on AC hydrogels. For the present work, we underline that the trend of the mesh size on passing from AC1 to AC6, rather than the absolute value of ξ, should be considered the key factor. Indeed the accurate evaluation of the mesh size is beyond the scope of the present investigation. Thus, the mesh sizes given in the last line of Table 1, decrease systematically on going from AC1 to AC6. ~~. In a previous work we also verified that the dimension of mesh sizes observed via TEM~~

~~analysis are in accordance with the calculated ones.~~

Table 1. Chemical composition and mesh size of the AC hydrogels obtained with the method described in ref. 80. . For the mesh sizes, standard deviations are given in parentheses.

	AC1	AC2	AC4	AC6
PBS [mL]	98.5	98.2	96.5	67.5
carbomer 974P [g]	0.5	0.5	0.5	0.5
agarose [g]	0.5	0.5	0.5	0.5
propylene glycol [mL]	-	0.3	1.5	30.0
glycerol [mL]	-	1.0	1.5	1.0
TEA [mL]	0.5	0.5	0.5	0.5
mesh size[a] ξ [nm]	44(8)	21(4)	12(3)	7(1)

[a] For the meaning of the absolute values of ξ reported here see discussion.

2.3 Ibuprofen release from AC hydrogels

Prior to release experiments, the hydrogel samples were swollen overnight, until equilibrium was reached in the isoconcentrated ibuprofen aqueous solution, so to limit the effect of mass-transfer processes associated with swelling phenomena. The contribution of matrix degradation was neglected, as the characteristic time of release (hours) is much smaller than the degradation time, which, according to our previous study [77], was estimated to be more than 1 month.

Three samples of gel loaded with an ibuprofen concentration of 30 mg mL^{-1} were put in excess PBS (to maintain a constant pH of 7.4) and stored at 37°C under a 5% CO2 atmosphere. Minimal aliquots were collected at defined time points, while the solution was refreshed, to avoid mass-transfer equilibrium between the gel and the surrounding PBS solution, exploiting the high concentration gradient as the driving force. The amount of released IBU was measured by UV absorption at λ = 264 nm.

2.4 NMR spectroscopy

The ^{1}H HR-MAS PGSE experiments on hydrogel samples were performed on a Bruker Avance spectrometer operating at 500 MHz proton frequency, equipped with a dual $^{1}H/^{13}C$ HR-MAS probe head for semi-solid samples. Samples were transferred in a 4 mm ZrO_2 rotor containing a volume of about 12 μL. A spinning rate of 4 kHz was used in all the experiments to eliminate the dipolar contribution. The PGSE experiments were performed using the bipolar pulse longitudinal eddy current delay (BPPLED) sequence. A pulsed gradient unit capable of producing magnetic field pulse gradients in the z-direction up to 53 $G*cm^{-1}$ was applied. The pulse gradients were

incremented from 2 to 95% of the maximum gradient strength in a linear ramp. For ibuprofen-loaded hydrogels, experimental data were collected at twelve different diffusion times, t_d, namely at 25, 35, 50, 60, 70, 80, 100, 120, 200, 250 and 300 ms, consequently the δ values were adjusted in the range of 3-0.7 ms to reach a good gradient optimization. In each experiment, a series of 32 spectra with 32k points and 16 scans was collected. The temperature was set and controlled at 32 °C with an air flow of 535 L×h^{-1}, to avoid temperature fluctuations due to sample heating during the magnetic field pulse gradients.

The ^{1}H high resolution PGSE experiments on the IBU-90 solution sample were performed on a Bruker Avance spectrometer operating at 500.13 MHz proton frequency equipped with a QNP four nuclei switchable probe. Experimental conditions similar to those described for the gel samples, such as the td values, number of scans and number of 2D experiments, were used for the solution sample.

3. Theory of diffusion and PGSE-NMR experiments

PGSE-NMR experiments allow the investigation of the translational molecular motions during a defined diffusion time t_d. The experimental technique relies on the application of magnetic pulsed field gradients (PFG) which encode and, later on, decode the molecular mean-square displacement (MSD) along the gradient direction (z-axis). The diffusion time t_d defines the time-scale of the NMR measurements. In isotropic systems, the MSD's along the three orthogonal axes are statistically equivalent and therefore we have:

$$\left\langle z^2(t)\right\rangle = \frac{1}{3}\left\langle \left(\mathbf{r}(t)-\mathbf{r}(0)\right)^2\right\rangle \tag{1}$$

where $\mathbf{r}(t)$ is the position of the tagged species at time t, $\mathbf{r}(0)$ is its starting position, and $\langle ... \rangle$ indicates an ensemble average.

In the q-space approach, the signal intensity $I(q,t_d)$, acquired through a series of experiments with variable gradient strength, is a function of the encoding time t_d and the reciprocal spatial vector q. This is defined as $q = (\delta\gamma g)/2\pi$ (in units of μm^{-1}), where γ is the magnetogyric ratio of the observed nucleus, g is the field gradient and δ is the gradient pulse. The signal decay $I(q,t_d)$ is related to the displacement probability average propagator $\overline{P}(z,t_d)$ [64-66] through a Fourier transform, according to the equation:

$$I(q,t_d) = I_0 \int_{-\infty}^{+\infty} \overline{P}(z,t_d) e^{iqz} dz \tag{2}$$

Fickian diffusion is characterized by a molecular MSD scaling linearly with time:

$$\left\langle z^2(t_d)\right\rangle = 2Dt_d \tag{3}$$

where D is the molecular diffusion coefficient (the factor 2 relates to the fact that we are monitoring diffusion along just one spatial direction). In the simplest case, *e.g.* for free and unrestricted diffusion in a homogenous and isotropic medium, the particle displacement distribution probability is Gaussian and given by:

$$P(z,t_d) = \sqrt{\frac{\pi}{Dt_d}} e^{-\frac{z^2}{4Dt_d}} \tag{4}$$

Applying Eq. (2), the experimental signal intensity $I(q,t_d)$ at the echo point becomes:

$$I(q,t_d) = I(0,t_d) e^{-q^2 Dt} \tag{5}$$

The numerical value of the diffusion coefficient can be extracted from the full width at half-maximum, $\Delta_{0.5}(t_d)$ of Eq. (5):

$$\Delta_{0.5}(t_d) = 2\left[4Dt_d \ln 2\right]^{1/2} \tag{6}$$

Equations (3-5) describe not only the free diffusion motion of low viscosity liquid samples, but also many diffusion processes occurring in the presence of obstacles or heterogeneities. An average Gaussian displacement distribution probability can be expected to emerge whenever the diffusion time and the mean diffusion distance (the square root of the molecules' MSD) become much larger than the characteristic time- and length-scales associated with these obstacles. Still, there are also many interesting situations characterized by an "anomalous diffusion" [81]. In these cases, the molecular MSD's may not increase linearly in time. Instead, one has [82]:

$$\left\langle z^2(t_d) \right\rangle \propto t_d^{\alpha} \tag{7}$$

In general there may be both a subdiffusive regime when the exponent is $0<\alpha<1$, and an enhanced or superdiffusive regime when $\alpha>1$. Clearly, ordinary Fickian diffusion is recovered for $\alpha=1$. Eq. (2) is completely general and remains valid even in the case of anomalous diffusion. The molecular displacement probability profiles can still be determined without any assumption, by performing the inverse Fourier transform of the experimental signal attenuation as a function of q. In these cases, the resulting $\overline{P}(z,t_d)$ is typically non-Gaussian.

A full understanding of the origin of anomalous diffusion phenomena can be obtained in the framework of the continuous time random walk (CTRW) model [83-86]. Eq. (7) can be derived from a fractional diffusion equation, describing the diffusion of particles potentially characterized by broad distributions in both space and time. In our notation, this equation can be written as:

$$\frac{\partial \overline{P}(z,t_d)}{\partial t} = D_t^{1-\beta} K_{\beta}^{\mu} D_z^{\mu} \overline{P}(z,t_d), \tag{8}$$

where D_z^{μ} is the Weyl operator describing a fractional space derivative, $D_t^{1-\beta}$ is a fractional time

derivative, and K_β^μ is a generalized diffusion coefficient having dimensions m^μ / s^β.

The solutions of Eq.(8) have been discussed elsewhere [82]. One remarkable and general property of such solutions is the time and space scaling. Given a pair of diffusion times t_1 and t_2, the following relation holds:

$$t_1^{-\beta/\mu}\overline{P}(zt_1^{-\beta/\mu}, t_1) = t_2^{-\beta/\mu}\overline{P}(zt_2^{-\beta/\mu}, t_2) \tag{9}$$

The exponents β and μ can be combined to give the exponent α of Eq.(7):

$$\alpha = \frac{2\beta}{\mu} \tag{10}$$

According to Eq.(9), the full width at half maximum should also scale as $t^{\alpha/2}$:[52]

$$\Delta_{0.5}(t_d) \propto t_d^{\alpha/2} \tag{11}$$

A generalized expression for the Fourier transform of the solutions of Eq.(8), which provides a very general model for the signal attenuation, is: [87,88]

$$I(q, t_d) = I(0, t_d)e^{-K_\beta^\mu t_d^\beta |q|^\mu} \tag{12}$$

The above equation can be applied to describe subdiffusive as well as superdiffusive processes. It should be noted that Eq.(12) has not been rigorously derived within the CTRW model, yet its functional form can be inferred considering the solutions of Eq.(8) for β<1 and μ=2 (representing commonly observed subdiffusion) and for β=1 and μ<2 (representing commonly observed superdiffusion) [82].

4. Results and discussion

4.1 PGSE NMR data analysis

We start our discussion by comparing of the raw PGSE-NMR signal attenuation data for the IBU-90 solution and the ibuprofen-loaded hydrogels. Free and unconstrained Gaussian diffusion is expected for the aqueous solution, leading to a linear drop of the logarithm of the signal intensity with q^2. Figure 1 compares the PGSE-NMR data collected for IBU-90 with those for AC6-90 at different diffusion times t_d. While the linear behavior expected for IBU-90 is effectively observed, deviations from linearity are evident at all times in the gel case. A similar non-linear drop in signal intensity can be observed also in the other samples, thereby suggesting the possibility of non-Gaussian diffusion of ibuprofen. Additional plots are provided in the SI.

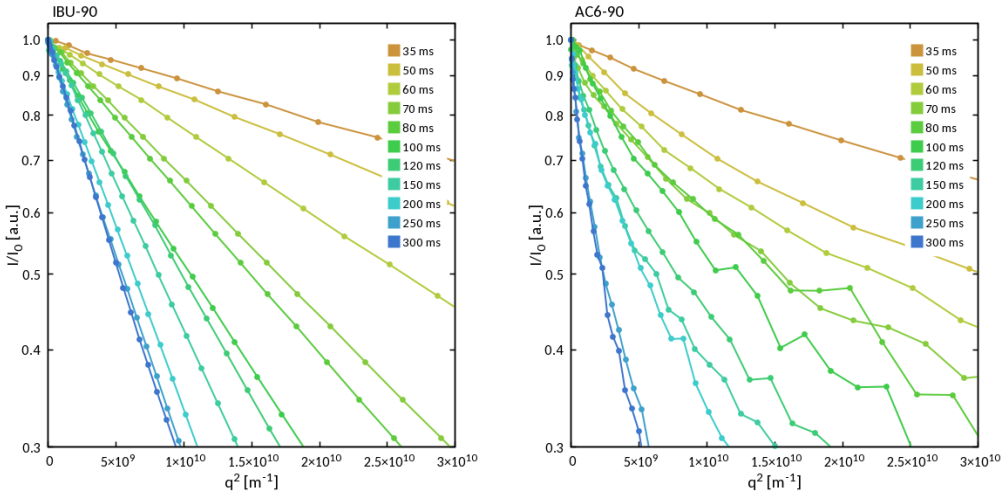

Fig. 1 Semilogarithmic plot of normalized NMR (I/I_0) signal intensity against q^2 for IBU-90 (left) and AC6-90 (right).

To clarify the nature of such deviations and characterize ibuprofen transport, NMR signals were analyzed according to the *q*-space approach (see above). The displacement distribution profiles, $\overline{P}(z,t_d)$, can be obtained by inverse Fourier transform. An example of such profiles is shown in Figure 2 (left panel) for AC2-60. Note that the reconstructed $\overline{P}(z,t_d)$ show some spurious oscillations, due to the sampling of a finite *q*-space interval. Note also that the typical molecular displacements are of the order of 10-100 μm, i.e. almost microscopic and much larger than the gel mesh sizes ξ given in Table 1. Analogous plots for the other samples indicated in all cases a displacement distribution widening over time.

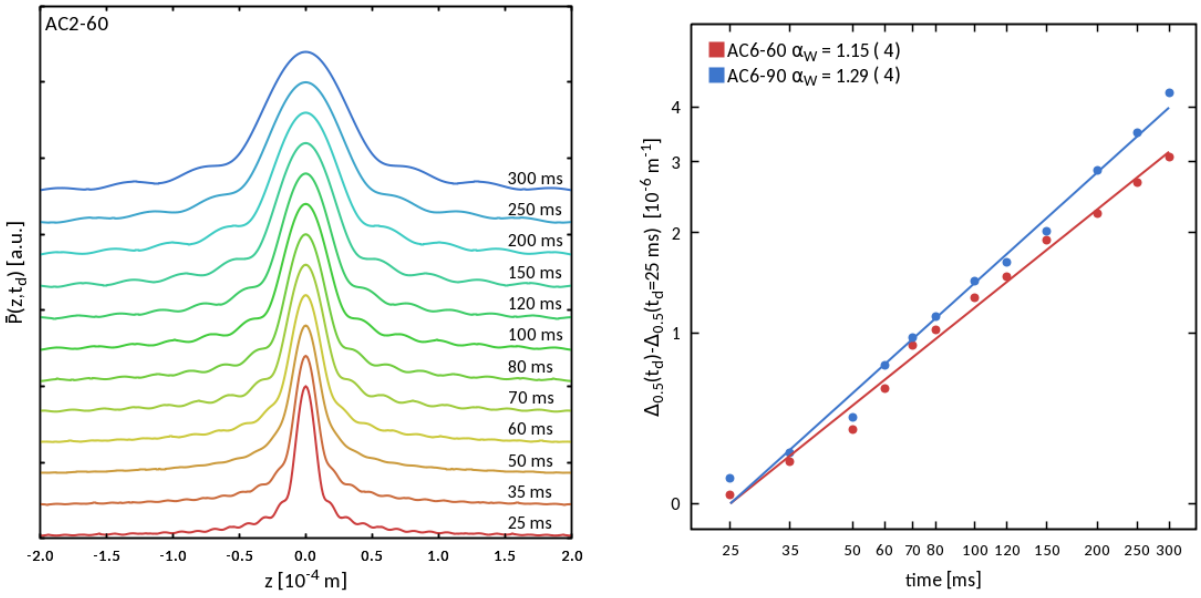

Fig. 2 Left: Displacement distribution profiles $\overline{P}(z,t_d)$ for AC2-60. Right: logarithmic plots of $\Delta_{0.5}(t_d)$ values extracted from $\overline{P}(z,t_d)$ (points). Lines represent fits to these points via Eq.(11). To facilitate the comparison of the slopes, the lines were shifted along the *y* direction by subtracting the smallest value, corresponding to t_d = 25 ms.

To quantify the widening of the distributions with time, we have extracted at each time t_d the full width at half maximum, $\Delta_{0.5}(t_d)$. According to Eq.(11), $\Delta_{0.5}(t_d)$ should scale as $t^{\alpha/2}$, where α is the fractional diffusion exponent defined in Eq.(7). A first estimate of α, α_W hereafter, is thus obtained by fitting $\Delta_{0.5}(t_d)$ to straight lines on a log-log scale. The procedure is illustrated in Figure 2 (right panel) for AC6-60 and AC6-90. Table 2 collects the values of α_W for all samples. We systematically find $\alpha_W \geq 1$, indicating a nearly Fickian or a mild superdiffusive behavior. A marked superdiffusive transport regime is observed in AC6-90 with α_W = 1.40(4), and AC6-120 with α_W = 1.44(9).

To confirm these findings, we have also estimated α by an approach based on the self-similar properties of the displacements profiles. According to Eq. (9), rescaling *z* to $z\,t_d^{-\alpha/2}$ should collapse the displacement distributions $\overline{P}(z,t_d)$ obtained at different times into the same function. The optimal value of α, α_S hereafter, corresponds to the minimum of the following function [52]:

$$S(\alpha) = \sum_{t_d} \frac{\int_{-\infty}^{+\infty} \left| \overline{P}_t(z,\alpha) - \overline{P}(z,t_d) \right| dz}{\int_{-\infty}^{+\infty} \overline{P}_t(z,\alpha) dz}, \qquad (13)$$

where $\overline{P}_t(z,\alpha)$ is the average distribution, obtained by averaging the rescaled $\overline{P}(z,t_d)$ over different correlation times. Figure 3 provides an example of $S(\alpha)$ profiles for IBU-90, AC2-90, and AC6-90. Similar profiles are obtained for the other samples. In all cases, the $S(\alpha)$ functions have a single minimum at a value $\alpha_S \geq 1$, allowing us to exclude the possibility of multiple transport regimes for the ibuprofen molecule.

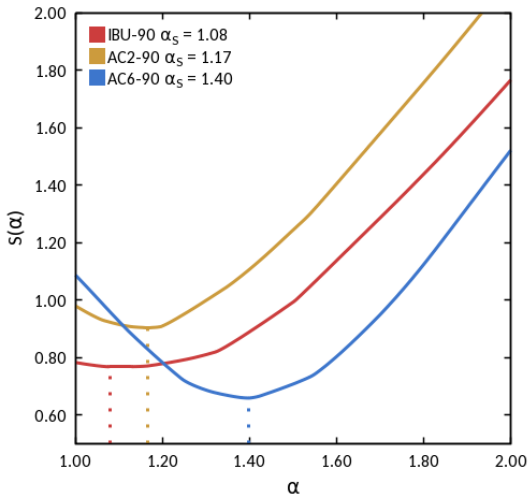

Fig. 3 Plots of $S(\alpha)$ (Eq.(13)) for IBU-90, AC2-90, and AC6-90. Projections of function minima on the α axis are shown as dotted lines.

Table 2 and Figure 4 collect all the measured α_W and α_S values for the hydrogels and the aqueous solution. Note the good agreement between the two values for each system, thus confirming their reliability. For simplicity, henceforth we shall use a single set of values and assume $\alpha=\alpha_S$. On the other hand, there is no clear correlation between α and the ibuprofen concentration, nor the gel structure, as measured by the mesh size ξ (see again Table 1). Nonetheless, the large α values obtained for samples AC6-90 and AC6-120 appear to be related to both the small mesh size and the relatively high ibuprofen concentration.

Table 2. Fractional diffusion exponents. The α_W label refers to the average value of α obtained for each sample by fitting $\Delta_{0.5}(t_d)$ values via Eq.(11). Standard deviations are reported in parentheses. The α_S values were obtained via the self-similarity approach described in the main text.

Sample	α_W	α_S
IBU-90	1.19(8)	1.22
AC1-60	1.26(5)	1.23
AC1-90	1.08(6)	1.14
AC1-120	1.14(5)	1.23
AC2-60	1.17(1)	1.17
AC2-90	1.19(14)	1.18
AC2-120	1.16(3)	1.15
AC4-60	1.09(3)	1.06
AC4-90	1.14(3)	1.18

AC4-120	1.19(3)	1.20
AC6-60	1.21(3)	1.20
AC6-90	1.40(4)	1.42
AC6-120	1.44(9)	1.55

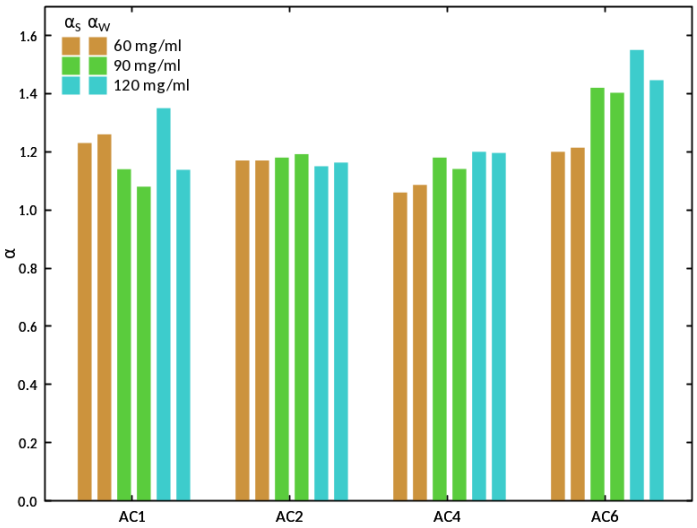

Fig. 4 Plot of α_W and α_S values of ibuprofen in gels AC1-AC6 at increasing ibuprofen concentrations.

The *q*-space analysis of PGSE-NMR data described so far was carried out without any *a priori* assumption about the underlying diffusion mechanisms or the functional form describing signal attenuation. The displacement distribution profiles were obtained by Fourier transforming raw NMR signals, which were then analyzed to extract α exponents. We now make one further step forward on the basis of the CTRW model of diffusion. In this model, particle motion is described as a random walk in both space and time, characterized by decoupled jump length and waiting time distribution functions. According Eq. (10), the α values are the ratios between the 2β and μ exponents introduced in Eq. (8). These reflect the waiting times (trapping) and the jump length (flow) of the drug molecule within the hydrogel, respectively. They are a manifestation of the structural and chemical complexity of the matrix, leading to heterogeneity in both the effective viscosity of the medium and in the drug-polymer interactions.

Our finding that in some samples α may be greater than unity implies $2\beta>\mu$ and, since $\beta\leq1$, also $\mu<2$. The value of α alone does not specify the relative contributions of β and μ to ibuprofen transport. In order to estimate them, the functions $\overline{P}(z,t_d)$ were fitted to the Fourier transforms of Eq. (12) for each time t_d. The values of α were those of α_S obtained via Eq.(13). We considered β and K_β^μ as free adjustable parameters, with the constraint that $0<\beta\leq1$ as required by the fractional

diffusion equation (Eq.(8)). At each t_d, the value of μ was determined from that of β and α via Eq. (10). This optimization strategy is expected to provide more accurate results than directly fitting the raw signal intensity to Eq. (12), as the displacement distribution profiles are much smoother than the original PGSE-NMR signals. The final values of β, K_β^μ were obtained by averaging over all times t_d. The confidence intervals for these parameters were calculated taking the mean standard deviations. Those of μ, were obtained via Eq. (10), assuming α constant. Table 3 collects the final values of β, K_β^μ and μ, along with the values of α (α_S see Table 2).

It should be noted that, within each given sample, increasing t_d negligibly affected the optimal values of these parameters. Hence, superdiffusive behavior persists up to the largest observation times.

Table 3. Numerical values of μ, β and K_β^μ calculated fitting $\overline{P}(z,t_d)$ to the Fourier transforms of Eq.(12). For better clarity, the values of α used in the fitting procedure (α_S see Table 2) are also reported.

Sample	$\alpha(=\alpha_S)$	μ	β	K_β^μ [m^μ/s^β]
IBU-90	1.22	1.64(2)	1.00(1)	3.33(8)E-8
AC1-60	1.23	1.24(8)	0.76(5)	3.45(13)E-6
AC1-90	1.14	1.23(15)	0.70(9)	2.83(12)E-6
AC1-120	1.23	1.35(8)	0.83(5)	1.19(3)E-6
AC2-60	1.17	1.49(7)	0.87(4)	1.68(1)E-7
AC2-90	1.18	1.05(15)	0.62(9)	2.10(19)E-5
AC2-120	1.15	0.98(10)	0.56(6)	3.61(15)E-5
AC4-60	1.06	1.30(18)	0.69(10)	1.04(4)E-6
AC4-90	1.18	1.40(23)	0.83(14)	3.65(11)E-7
AC4-120	1.20	1.67(2)	1.00(1)	1.26(31)E-8
AC6-60	1.20	1.64(5)	0.98(3)	2.32(1)E-8
AC6-90	1.42	1.36(7)	0.97(5)	8.98(15)E-7
AC6-120	1.55	1.29(1)	1.00(1)	1.12(7)E-6

The values of the space fractional parameter μ are collected in graphical form in Figure 5. According to the CTRW approach, small values of μ can be associated with the possibility of large molecular displacements or “jumps” with heavy-tailed length distributions (Levy flights) [53,54]. In our samples, the values of μ span a large interval, from 0.98 to 1.67. However, our estimates of μ revealed no direct correlation with AC gel mesh size or drug concentration.

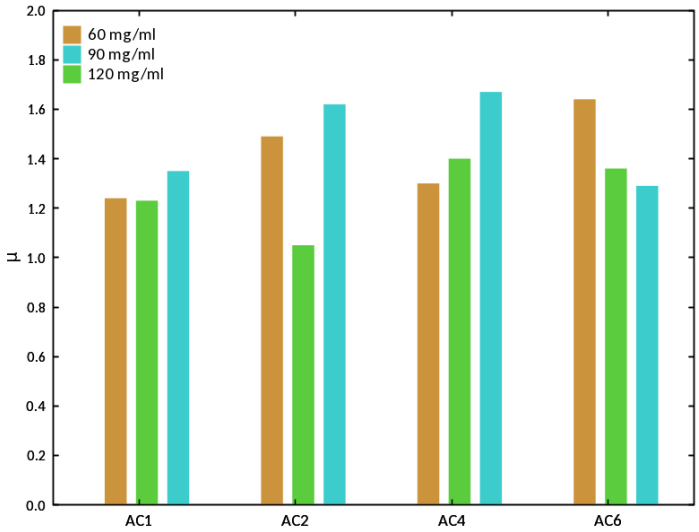

Fig. 5 Plots of the μ values of ibuprofen in gels AC1, AC2, AC4 and AC6 at increasing concentration 60 mg/mL, 90 mg/mL and 120 mg/mL.

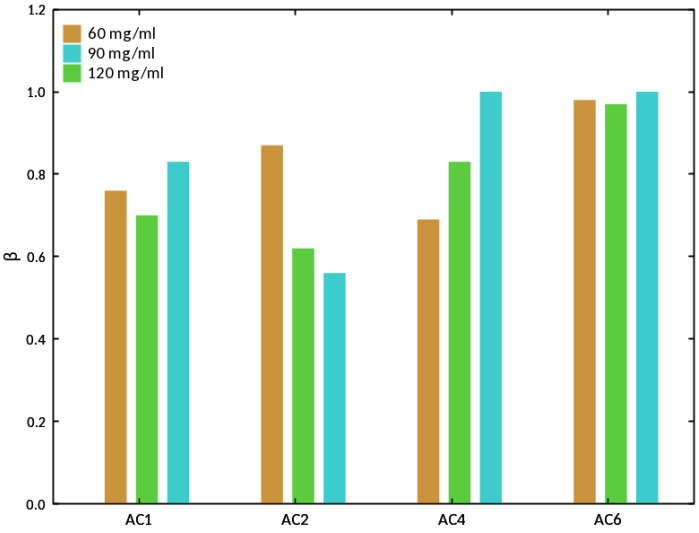

Fig. 6 Plots of the β values of ibuprofen in gels AC1, AC2, AC4 and AC6 at increasing concentration 60 mg/mL, 90 mg/mL and 120 mg/mL.

Figure 6 collects the values of the time fractional parameter β of the gel samples at increasing ibuprofen concentration. The value of β depends on the behavior of the diffusing species in the time domain. Small β values (β<1), associated with broad distributions of waiting times, likely indicate that the diffusing molecules remain temporarily trapped within the hydrogel pores or form strong physical association with the polymer chains. Ibuprofen loaded in AC hydrogels experiences broadly distributed resting times (β value in the range 0.64-1) within the observed

spatiotemporal window. The β exponent appears to be sensitive primarily to gel pore dimensions and then to drug concentration.

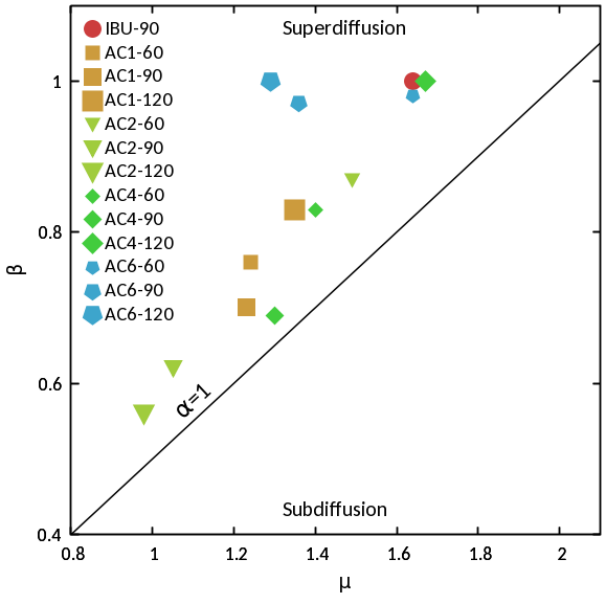

Fig. 7 Diagram of β *vs* μ for AC gel at variable mesh size and increasing drug concentration. The line 2β=μ represents Fickian diffusion, for which α =1.

Figure 7 summarizes the results of our PFGE-NMR data analysis. On this scatter plot, the line 2β=μ corresponds to Fickian diffusion (α=1) and separates the superdiffusion and subdiffusion regimes (above and below, respectively) [82]. All samples fall in the upper half of the diagram. In some systems, such as AC1-90, AC2-90, AC2-120, and AC4-60 a nearly Fickian diffusion regime is recovered. In these gel systems, the competition between long trapping times and large jumps results in a MSD increasing linearly in time, thus hiding the anomalous character of the diffusive motion.

4.2 Drug release behavior

So far, we have analyzed ibuprofen diffusion on a microscopic length (10-100 μm) and time (25-300 ms) scales via NMR spectroscopy. At this point, to understand the implications of previous results in the context of macroscopic diffusion, we performed release experiments on ibuprofen-loaded hydrogels. As specified above, the initial ibuprofen concentration in such experiments was 30 mg/mL. Figure 8 shows the fractional normalized release profiles as a function of time. Taking into account the shape of our hydrogel samples, we fitted the release data with a model equation describing drug release from a cylindrical sample. Assuming the drug molecules homogeneously

distributed within the polymer matrix, the exact solution of the Fick's second law can be written as a function of the fractional drug release, M_t/M_∞ (see Eq. (15) of Ref. 32):

$$\frac{M_t}{M_\infty} = 1 - \frac{32}{\pi^2}\sum_{n=1}^{\infty}\frac{1}{q_n^2} exp\left(-\frac{q_n^2}{R^2}Dt\right)\sum_{l=0}^{\infty}\frac{1}{(2l+1)^2} exp\left(-\frac{(2l+1)^2\pi^2}{H^2}Dt\right) \qquad (14)$$

where, M_t and M_∞ are the cumulative amounts of drug released at time t and at infinite time, respectively.

R and H represent the radius and height of the cylinder, here 5.2 and 18.3 mm, respectively. D is the diffusion coefficient of the drug within the system, while q_ns are the roots of the zero order Bessel function $J_0(Rq_n) = 0$. Data fitting [89] was performed by truncating both series at n, l = 10.

Figure 8 shows the result of the fitting procedure, where only the diffusion coefficient, D, was used as fitting parameter. Optimal D values are reported in Table 4, along with their standard deviations. Their magnitude decreased with decreasing mesh size, consistently with the idea that ibuprofen release rate is proportional to the accessibility of water-filled regions, here qualitatively represented by the mesh size.

The coefficients were obtained from the adoption of Eq. (14), which represents the solution of the Fick's second law for a cylindrical geometry, cannot be directly compared with the generalized diffusion constants obtained from the fractional diffusion equation (Eq. (8)).

Besides, the standard deviations in Table 4 suggest that Eq. (14) adequately describes ibuprofen release from the hydrogel matrix. This is not surprising, considering that Lèvy distributions can be expected to develop over time the same long-distance behavior of Gaussian distributions [90]. As noted elsewhere [46], the crossover from a non-Gaussian to a Gaussian distribution can exceed experimentally accessible times. Based on the results presented so far, we argue that the time scale spanned by release experiments (hours) may be large enough for the crossover to occur. Further investigations, probing intermediate time scales, will help identifying the onset of Gaussian diffusion and the relationship between microscopic and macroscopic diffusion regimes. We stress that ibuprofen diffusion at the NMR scale cannot be interpreted as Gaussian, and this is univocally demonstrated by the signal decay behavior (see Figure 1).

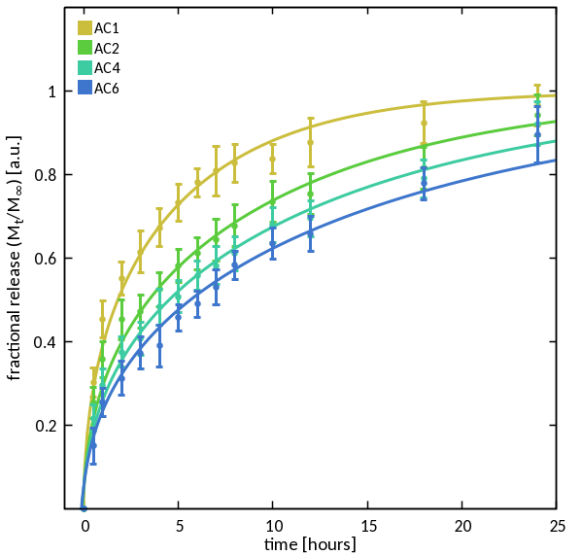

Fig. 8 Fractional normalized drug release (M_t/M_∞) profiles (points) for all hydrogels loaded with 30 mg/mL ibuprofen. Lines represent fits to the data using the cylindrical model for monolithic solutions (see Eq.(15) in Ref. 32).

Table 4. Diffusion coefficients (*D*) of ibuprofen obtained from fitting the release data via Eq.(14).

Sample	D [10^{-11}m^2/s]
AC1	17.9(8)
AC2	9.4(4)
AC4	7.1(3)
AC6	5.7(3)

4.3 Molecular transport mechanisms

Anomalous superdiffusive processes, which can be described in terms of the CTRW model and Lévy flights, have been extensively studied theoretically, [91] yet experimental evidence of this motion regime in soft materials is far less common. [49,54,92] A major difficulty is represented by the characterization of the chemical interactions that are responsible for the observed behavior. Based on our previous works, [63] we identify these chemical interactions in hydrogen bonding between the agarose hydroxyl groups and ibuprofen carboxylate moiety. The strength of these interactions and their impact on ibuprofen motion greatly vary from one sample to another.

Despite the absence of a clear-cut correlation between mesh size, or ibuprofen concentration, and the diffusion exponents due to sample heterogeneity, some general trends can be extracted from our results, which can be used to develop a model describing ibuprofen diffusion. In hydrogels AC1,

AC2, and AC4 (except AC4-120) ibuprofen transport regime results from the combination of two factors. First, the long waiting times ($\beta < 1$) associated with ibuprofen trapping in accessible sites formed by the polymer network. Second, the large spatial displacements ($\mu < 2$), which occur during ibuprofen detrapping and release in bulk water. For the remaining samples (AC6-60, AC6-90, AC6-120, and AC4-120), the value of β approaches unity, suggesting that trapping plays a minor role on diffusion dynamics upon decreasing the mesh size. The deviations from the Fickian behavior depend entirely on the spatial domain ($\mu < 2$). The mechanism so far described appears consistent with our previous studies [63] and similar to the Lèvy models developed to describe molecular dynamics at the liquid-solid interface. [49,92] A final remark concerns our results for ibuprofen in solution (IBU-90). In contrast our original expectations, the diffusion exponent μ differs from that associated with free unconstrained, Gaussian diffusion ($\mu = 2$). This outcome is likely due the clustering of ibuprofen molecules in solution, which ultimately affect the NMR decay signal.

5 Conclusions

We have reported a combined experimental and theoretical investigation on ibuprofen transport in agarose-carbomer hydrogels, considering samples with varying nanoscopic mesh size and drug concentration. In many of them, the analysis of experimental NMR data has evidenced superdiffusive ibuprofen transport. These features, generally associated with deviations from the ordinary Fickian behaviour, have been interpreted in terms of the fractional diffusion model, with the aim of clarifying the separate roles of the time and space domains. Our analysis has shown that, even in case of modest deviations from the Fickian behaviour, the diffusion dynamics is characterized by a broad distribution of spatial “jumps” (Lèvy flights), due to the combination of trapping-detrapping events related to the formation and breaking of hydrogen bonds between ibuprofen and the hydrogel matrix.

Although not systematically, we have found a correlation between the hydrogel mesh size and the onset the superdiffusive transport regime, essentially due to the restoration of a linear diffusive regime in the time domain. We point out that, although the notion of anomalous diffusion in these systems has emerged in some recent works, [50,51] the application of Lèvy transport models to drug transport in hydrogels has never been attempted before.

In order to assess the implications of our findings on a macroscopic time scales, we release data were fitted with a model describing drug release from a cylindrical sample. The resulting diffusion coefficients decreased by decreasing the mesh size. We also found this model, which conform to Fick’s second law, to adequately describe release data. This outcome suggests that the time scale of release experiments might be large enough for superdiffusive diffusion to turn into ordinary Fickian

diffusion, which is expected to occur for sufficiently long times [46,90]. Based on the results so far presented, the crossover between Lèvy and Gaussian distribution may take place at intermediate time scales, which could not be accessed in this work.

In the next future, we plan to investigate the diffusion of molecular species other than ibuprofen in AC hydrogels, thus extending the validity of our findings to other systems. As done in our previous work on ionic liquids [93], we will combine theoretical and experimental approaches to establish a more quantitative connection between microscopic diffusion and drug release. As noticed above, this will possibly require the adoption of additional experimental techniques able to bridge the gap between solute transport mechanisms and release kinetics.

Acknowledgements

FC, MC and GR acknowledge the financial support of PRIN 2015, project no. 2015XJA9NT 003 "Molecular Organization in Organic Thin Films via Computer Simulation of their Fabrication Processes".

Supplementary data

Supplementary data to this article can be found online at …..

References

[1] L. Voorhaar and R. Hoogenboom, Supramolecular polymer networks: hydrogels and bulk materials, *Chem. Soc. Rev*. 45 (2016) 4013-4031.

[2] X. Du, J. Zhou, J. Shi, and B. Xu, Supramolecular hydrogelators and hydrogels: from soft matter to molecular biomaterials, *Chem. Rev.* 115 (2015) 13165-13307.

[3] M. Mahinroosta, Z. J. Farsangi, A. Allahverdi, Z. Shakoori, Hydrogels as intelligent materials: a brief review of synthesis, properties and applications, *Materials Today Chemistry* 8 (2018) 42-55.

[4] D. Caccavo, S. Cascone, G. Lamberti, A. A. Barba, and A. Larsson, Drug delivery from hydrogels: a general framework for the release modeling, *Curr. Drug Deliv.* 14 (2) (2017) 179-189.

[5] L. T. A. Hong, Y-M. Kim, H. H. Park, D. H. Hwang, Yu. Cui, E. M. Lee, S. Yahn, J. K. Lee, S-C. Song, B. G. Kim, An injectable hydrogel enhances tissue repair after spinal cord injury by promoting extracellular matrix remodelling, *Nat. Comm*., 8 (2017) 533.

[6] H. R. Culver, M. E. Wechsler, and N. A. Peppas, Label-free detection of tear biomarkers using hydrogel-coated gold nanoshells in a localized surface plasmon resonance-based biosensor, *ACS Nano* 12 (2018) 9342-9354.

[7] J-W. Seo, H. Kim, K. Kim, S. Q. Choi, and H. J. Lee, Calcium-modified silk as a biocompatible and strong adhesive for epidermal electronics *Adv. Funct. Mater.* 28 (2018) 1800802.

[8] H. J. van der Linden, S. Herber, W. Olthuisa and P. Bergveld, Stimulus-sensitive hydrogels and their applications in chemical (micro)analysis, *Analyst* 128 (2003) 325-331.

[9] K. M. Raju and M. P. Raju, Synthesis of novel superabsorbing copolymers for agricultural and horticultural applications *Polym. Int.* 50 (2001) 946-951.

[10] M. E. Caldorera-Moore, W. B. Liechty, and N. A. Peppas, Responsive theranostic systems: integration of diagnostic imaging agents and responsive controlled release drug delivery carriers, *Acc. Chem. Res*. 44 (2011) 1061-1070.

[11] Y. Li, J. Rodrigues and H. Tomas, Injectable and biodegradable hydrogels: gelation, biodegradation and biomedical applications, *Chem. Soc. Rev*. 41 (2012) 2193-2221.

[12] S. Shukla and A. Shukla, Tunable antibiotic delivery from gellan hydrogels, *J. Mater. Chem. B* 6 (2018) 6444-6458.

[13] J. Mayr, C. Saldıas and D. Diaz, Release of small bioactive molecules from physical gels, *Chem. Soc. Rev*. 47 (2018) 1484-1515.

[14] D. Das and S. Pal, Modified biopolymer-dextrin based crosslinked hydrogels: application in controlled drug delivery, *RSC Adv*. 5 (2015) 25014-25050.

[15] J. Li and D. J. Mooney, Designing hydrogels for controlled drug delivery, *Nature Reviews Materials* 1 (2016) 16071.

[16] Y. S. Zhang and A. Khademhosseini, Advances in engineering hydrogels, *Science* 356 (2017) eaaf3627.

[17] H. R. Culver, J. R. Clegg, N. A. Peppas, Analyte-responsive hydrogels: intelligent materials for biosensing and drug delivery, *Acc. Chem. Res*. 50 (2) (2017) 170-178.

[18] X. Le, W. Lu, J. Zheng, D. Tong, N. Zhao, C. Ma, H. Xiao, J. Zhang, Y. Huang and T. Chen, Stretchable supramolecular hydrogels with triple shape memory effect, *Chem. Sci*. 7 (2016) 6715-6720.

[19] M. Ikeda, R. Ochi, A. Wada and I. Hamachi, Supramolecular hydrogel capsule showing prostate specific antigen-responsive function for sensing and targeting prostate cancer cells, *Chem. Sci*. 1 (2010) 491-498.

[20] N. Oliva, J. Conde, K. Wang, and N. Artzi, Designing hydrogels for on-demand therapy, *Acc. Chem. Res*. 50 (2017) 669-679.

[21] N. Joshi, J. Yan, S. Levy, S. Bhagchandani, K. V. Slaughter, N. E. Sherma, J. Amirault, Y. Wang, L. Riegel, X. He, T. S. Rui, M. Valic, P. K. Vemula, O. R. Miranda, O. Levy, E. M. Gravallese, A. O. Aliprantis, J. E. J. M. Karp, Towards an arthritis flare-responsive drug delivery system, *Nat. Comm*. 9 (2018) 1275.

[22] K. H. Bae, L-S. Wang and M. Kurisawa, Injectable biodegradable hydrogels: progress and challenges, *J. Mater. Chem. B* 1 (2013) 5371-5388.

[23] Y. Liu, Y. Sui, C. Liu, C. Liu, M. Wu, B. Li, Y. Li, A physically crosslinked polydopamine/nanocellulose hydrogel as potential versatile vehicles for drug delivery and wound healing, *Carbohydrate Polymers* 188 (2018) 27-36.

[24] C. Ghobril and M. W. Grinstaff, The chemistry and engineering of polymeric hydrogel adhesives for wound closure: a tutorial, *Chem. Soc. Rev*. 44 (2015) 1820-1835.

[25] M. D. Konieczynska and M. W. Grinstaff, On-demand dissolution of chemically cross-linked hydrogels, *Acc. Chem. Res*. 50 (2017) 151-160.

[26] N. Kamaly, B. Yameen, J. Wu, and O. C. Farokhzad, Degradable controlled-release polymers and polymeric nanoparticles: mechanisms of controlling drug release, *Chem. Rev*. 116 (2016) 2602-2663.

[27] H. Komatsu, S. Matsumoto, S. Tamaru, K. Kaneko, M. Ikeda, and I. Hamachi, Supramolecular hydrogel exhibiting four basic logic gate functions to fine-tune substance release, *J. Am. Chem. Soc*. 131 (2009) 5580-5585.

[28] T. Shirakura, T. J. Kelson, A. Ray, A. E. Malyarenko, and R. Kopelman, Hydrogel nanoparticles with thermally controlled drug release, *ACS Macro Lett*. 3 (2014) 602-606.

[29] D. Seliktar, Designing cell-compatible hydrogels for biomedical applications, *Science* 336 (2012) 1124-1128.

[30] D. Caccavo, S. Cascone , G. Lamberti, A. A. Barba, Controlled drug release from hydrogel-based matrices: Experiments and modeling, *Int. J. Pharm.* 486 (2015) 144-152.

[31] N. A. Peppas, B. Narasimhan, Mathematical models in drug delivery: How modeling has shaped the way we design new drug delivery systems, *J. Control Release* 190 (2014) 75-81.

[32] J. Siepmann, F. Siepmann, Modeling of diffusion controlled drug delivery, *J. Control Release* 161 (2012) 351-362.

[33] D. Caccavo, S. Cascone, G. Lamberti, and A. A. Barba, Modeling the drug release from hydrogel-based matrices, *Mol. Pharmaceutics* 12 (2015) 474-483.

[34] W. I. Higuchi, Analysis of data on the medicament release from ointments, *J. Pharm. Sci*. 51 (1962) 802-804.

[35] J. Siepmann and N. A. Peppas, Higuchi equation: Derivation, applications, use and misuse, *Int. J. Pharm.* 418 (2011) 6-12.

[36] P. Gao and P. E. Fagerness, Diffusion in HPMC gels. I. Determination of drug and water diffusivity by pulsed-field-gradient spinecho NMR, *Pharm. Res.* 12 (1995) 955-964.

[37] T. G. Meikle, S. Yao, A. Zabara, C. E. Conn, C. J. Drummond and F. Separovic, Predicting the release profile of small molecules from within the ordered nanostructured lipidic bicontinuous cubic phase using translational diffusion coefficients determined by PFG-NMR, *Nanoscale* 9 (2017) 2471-2478.

[38] J. Bastide and S. J. Candau, in *Physical Properties of Polymer Gels*, edited by J. P. Cohen Addad, John Wiley and Sons, 1996.

[39] B. Amsdem, Solute diffusion within hydrogels. Mechanisms and models, *Macromolecules* 31 (1998) 8382-8395.

[40] S. Panyukov and Y. Rabin, Polymer Gels: Frozen inhomogeneities and density fluctuations, *Macromolecules* 29 (1996) 7960-7975.

[41] D. Hernández, F. Ramírez-Alatriste, J.C.R. Romo-Cruz, L. Olivares-Quiroz, Hydrodynamic dispersion in heterogeneous anisotropic porous media: A simple model for anomalous diffusion emergence, *Physica A* 508 (2018) 424-433.

[42] Y. Zhou, J. Li, Y. Zhang, D. Dong, E. Zhang, F. Ji, Z. Qin, J. Yang, and F. Yao, Establishment of a physical model for solute diffusion in hydrogel: understanding the diffusion of proteins in poly(sulfobetaine methacrylate) hydrogel, *J. Phys. Chem. B* 121 (2017) 800-814.

[43] G. S. Offeddu, E. Axpe, B. A. C. Harley, and M. L. Oyen, Relationship between permeability and diffusivity in polyethylene glycol hydrogels, *AIP Adv*. 8 (2018) 105006.

[44] F. Rossi, F. Castiglione, M. Ferro, P. Marchini, E. Mauri, M. Moioli, A. Mele, and M. Masi, Drug-Polymer interactions in hydrogel-based drug delivery systems: experimental and theoretical study, *Chem. Phys. Chem*. 16 (2015) 2818-2825.

[45] J. A. Ferreira, M. Grassi, E. Gudiño, P. de Oliveira, A new look to non-Fickian diffusion, *Appl. Math.l Model*. 39 (2015) 194-204.

[46] B. Wang, J. Kuo, S. C. Bae and S. Granick, When Brownian diffusion is not Gaussian, *Nature Mat*. 11 (2012) 481-485.

[47] J. Guan, B. Wang, and S. Granick, Even hard-sphere Colloidal suspensions display Fickian yet non-Gaussian diffusion, *ACS Nano* 8 (2014) 3331-3336.

[48] S. B. Alves, G. F. de Oliveira, L. C. de Oliveira, T. Passerat de Silans, M. Chevrollier, M. Oriá, H. L. D. de S. Cavalcante, Characterization of diffusion processes: normal and anomalous regimes, *Physica A* 447 (2016) 392-401.

[49] C. Yu, J. Guan, K. Chen, S. C. Bae, and S. Granick, Single-molecule observation of long jumps in polymer adsorption, *ACS Nano* 7 (2013) 9735-9742.

[50] S. Tang, M. Wang, and B. D. Olsen, Anomalous self-diffusion and sticky rouse dynamics in associative protein hydrogels *J. Am. Chem. Soc*. 137 (2015) 3946-3957.

[51] B. Stempfle, A. Große, B. Ferse, K.-F. Arndt, and D. Wöll, Anomalous diffusion in thermoresponsive polymer-clay composite hydrogels probed by wide-field fluorescence microscopy, *Langmuir* 30 (2014) 14056-14061.

[52] Y. Sagi, M. Brook, I. Almog, and N. Davidson, observation of anomalous diffusion and fractional self-similarity in one dimension, *Phys. Rev. Lett*. 108 (2012) 093002.

[53] P. Barthelemy, J. Bertolotti & D. S. Wiersma, A Lévy flight for light, *Nat. Lett.* 453 (2008) 495-498.

[54] M. S. Song, H. C. Moon, J.-H. Jeon, and H. Y. Park, Neuronal messenger ribonucleoprotein transport follows an aging Lévy walk, *Nat. Comm.* 9 (2018) 1-8.

[55] A. Bertz, J.-E. Ehlers, S. Wohl-Bruhn, H. Bunjes, K.-H. Gericke, H. Menzel, Mobility of green fluorescent protein in hydrogel-based drug-delivery systems studied by anisotropy and fluorescence recovery after photobleaching, *Macromol. Biosci.* 13 (2013) 215-226.

[56] F. Brandl, F. Kastner, R. M. Gschwind, T. Blunk, J. Teßmar, A. Göpferich, Hydrogel-based drug delivery systems: comparison of drug diffusivity and release kinetics, *J. Control. Release* 142 (2010) 221-228.

[57] M. Henke, F. Brandl, A. M. Goepferich, J. K. Tessmar, Size-dependent release of fluorescent macromolecules and nanoparticles from radically cross-linked hydrogels, *Eur. J. Pharm. Biopharm.* 74 (2010) 184-192.

[58] S. P. Zustiak, H. Boukaribc and J. B. Leach, Solute diffusion and interactions in cross-linked poly(ethylene glycol) hydrogels studied by Fluorescence Correlation Spectroscopy, *Soft Matter* 6 (2010) 3609-3618.

[59] S. M. Evans, A. L. Litzenberger, A. E. Ellenberger, J. E. Maneval E. L. Jablonski, B. M. Vogel, A microfluidic method to measure small molecule diffusion in hydrogels, *Mater. Sci. Eng. C* 35 (2014) 322-334.

[60] S. Lehmann, S. Seiffert, and W. Richtering, Spatially Resolved Tracer Diffusion in Complex Responsive Hydrogels *J. Am. Chem. Soc*. 134 (2012) 15963-15969.

[61] A. Pedacchia, A. Adrover, Study of release kinetics and diffusion coefficients in swellable cellulosic thin films by means of a simple spectrophotometric technique, *Chem. Eng. Res. Des.* 92 (2014) 2550-2556.

[62] M. D. Mantle, NMR and MRI studies of drug delivery systems, *Curr. Opin. Colloid Interface Sci.* 18 (2013) 214-227.

[63] F. Rossi, F. Castiglione, M. Salvalaglio, M. Ferro, M. Moioli, E. Mauri, M. Masi, A. Mele, On the parallelism between the mechanisms behind chromatography and drug delivery: the role of interactions with a stationary phase, *Phys. Chem. Chem. Phys*. 19 (2017) 11518-11528.

[64] *(a)* P. T. Callaghan, C. D. Eccles, Y. J. Xia, NMR microscopy of dynamic displacements: k-space and q-space imaging *Phys. E* 21 (2017) 820-822. *(b)* P. T. Callaghan, Principles of nuclear resonance microscopy, Oxford University Press, Oxford. U.K., 1991.

[65] D. G. Cory, A. N. Garroway, Measurement of translational displacement probabilities by NMR: an indicator of compartmentation, *Magn. Reson. Med*. 14 (1990) 435-444.

[66] Y. Cohen, Y. Assaf, High b-value q-space analyzed diffusion-weighted MRS and MRI in neuronal tissues - a technical review, *NMR Biomed*. 15 (2002) 516-542.

[67] D. Shishmarev, K. I. Momot and P. W. Kuchel, Anisotropic diffusion in stretched hydrogels containing erythrocytes: evidence of cell-shape distortion recorded by PGSE NMR spectroscopy, *Magn. Reson. Chem* .55 (2017) 438-446.

[68] C. Di Meo, T. Coviello, P. Matricardi, F. Alhaique, D. Capitani and R. Lamanna, Anisotropic enhanced water diffusion in scleroglucan gel tablets, *Soft Matter* 7 (2011) 6068-6075.

[69] M. Santoro, P. Marchetti, F. Rossi, G. Perale, F. Castiglione, A. Mele, M. Masi, Smart approach to evaluate drug diffusivity in injectable agar-carbomer hydrogels for drug delivery, *J. Phys. Chem. B* 115 (2011) 2503-2510.

[70] J. E. Jenkins, M. R. Hibbs, T. M. Alam, Identification of multiple diffusion rates in mixed solvent anion exchange membranes using high resolution MAS NMR, *ACS Macro Lett.* 1 (2012) 910-914.

[71] J. Chin, A. Chen, M. J. Shapiro, Improved high-resolution diffusion filtered ^{1}H MAS NMR, *Magn. Reson. Chem.* 38 (2000) 782-784.

[72] T. M. Alam, M. R. Hibbs, Characterization of heterogeneous solvent diffusion environments in anion exchange membranes, *Macromolecules* 47 (2014) 1073-1084.

[73] F. Rossi, X. Chatzistavrou, G. Perale, A. R. Boccaccini, Synthesis and degradation of agar -carbomer ba hydrogels for tissue engineering applications, *J. Appl. Polym. Sci.* 123 (2012) 398-408.

[74] Q. Wang, X. Q. Jin, J. H. Sun, S. Y. Bai, X. Wu, PAA-grafted surface and fractal feature of dense nanosilica spheres for ibuprofen delivery, *Mater. Chem. Phys.* 195 (2017) 213-223.

[75] S. Mongkolkitikula, N. Paradeeb, A. Sirivat, Electrically controlled release of ibuprofen from conductive poly(3-methoxydiphenylamine)/crosslinked pectin hydrogel, *Eur. J. Pharm. Sci.* 112 (2018) 20-27.

[76] A. Agostini, U. Capasso Palmiero, S. D. A. Barbieri, M. Lupi and D. Moscatelli, Synthesis and characterization of pH-sensitive drinkable nanoparticles for oral delivery of ibuprofen, *Nanotechnology* 29 (2018) 225604.

[77] Ilaria Caron, Filippo Rossi, Simonetta Papa, Rossella Aloe, Marika Sculco, Emanuele Mauri, Alessandro Sacchetti, Eugenio Erba, Nicolò Panini, Valentina Parazzi, Mario Barilani, Gianluigi Forloni, Giuseppe Perale, Lorenza Lazzari, Pietro Veglianese, A new three dimensional biomimetic hydrogel to deliver factors secreted by human mesenchymal stem cells in spinal cord injury, *Biomaterials* 75 (2016) 135-147.

[78] G. Perale, F. Rossi, M. Santoro, P. Marchetti, A. Mele, F. Castiglione, E. Raffa, M. Masi, Drug release from hydrogel: a new understanding of transport phenomena, *J. Biomed. Nanotechnol*. 7 (2011) 476-481.

[79] P. J. Flory, “Principles of Polymer Chemistry”, Cornell University Press.

[80] F. Rossi, G. Perale, G. Storti, and M. Masi, A library of tunable agarose carbomer -based hydr tissue engineering applications: The role of cross *J. Appl. Polym. Sci.* 123 (2012) 2211-2221.

[81] E. O. Stejskal, J. E. Tanner, Spin diffusion measurements: spin echoes in the presence of a time -dependent field gradient, *J. Chem. Phys*. 42 (1965) 288-291.

[82] R. Metzler, J. Klafter, The random walk's guide to anomalous diffusion: a fractional dynamics approach, *Phys. Rep.* 339 (2000) 1-77.

[83] H. Scher and M. Lax, Stochastic transport in a disordered solid. I. Theory, *Phys. Rev. B*, 7 (1973) 4491-4502.

[84] J. Klafter and R. Silbey, Derivation of the continuous-time random-walk equation, *Phys. Rev. Lett*., 44 (1980) 55-58.

[85] E. W. Montroll, G. H. Weiss, Random walks on lattices. II, *J. Math. Phys*., 6 (1965) 167-181.

[86] M. Kenkre, E. W. Montroll, M. F. Shlesinger, Generalized master equations for continuous-time random walks, *J. Stat. Phys.* 9 (1973) 45-50.

[87] Y. Fan and J.-H. Gao, Fractional motion model for characterization of anomalous diffusion from NMR signals, *Phys. Rev. E* 92 (2014) 012707.

[88] G. Lin, Analyzing signal attenuation in PFG anomalous diffusion via a modified Gaussian phase distribution approximation based on fractal derivative model, *Physica A* 467 (2017) 277-288.

[89] T. Williams, C. Kelley et al. Gnuplot 4.6: an interactive plotting program, http://gnuplot.sourceforge.net/ (last accessed: April 2019).

[90] C. Tsallis, S. Levy, A. Souza, R. Maynard, Statistical-mechanical foundation of the ubiquity of Lévy distributions in nature, *Phys. Rev. Lett.* 75 (1995) 3589-3593.

[91] R. Jain and K. L. Sebastian, Lévy flight with absorption: A model for diffusing diffusivity with long tails, *Phys. Rev. E* 95 (2017) 032135.

[92] M. J. Skaug, J. Mabry, J. and D. K. Schwartz, Intermittent molecular hopping at the solid-liquid interface, *Phys. Rev. Lett.* 110 (2013) 256101.

[93] M. Casalegno, G. Raos, G. B. Appetecchi, S. Passerini, F. Castiglione, and A. Mele, From nanoscale to microscale: crossover in the diffusion dynamics within two pyrrolidinium-based ionic liquids, *J. Phys. Chem. Lett.* 8 (2017) 5196-5202.